Integrated Discrete/Continuum Topology Optimization Framework for Stiffness or Global Stability of High-Rise Buildings

Lauren L. Beghini, Ph.D.[1]; Alessandro Beghini, M.ASCE[2]; William F. Baker, F.ASCE[3]; and Glaucio H. Paulino, M.ASCE[4]

Abstract: This paper describes an integrated topology optimization framework using discrete and continuum elements for buckling and stiffness optimization of high-rise buildings. The discrete (beam/truss) elements are optimized based on their cross-sectional areas, whereas the continuum (polygonal) elements are concurrently optimized using the commonly known density method. Emphasis is placed on linearized buckling and stability as objectives. Several practical examples are given to establish benchmarks and illustrate the proposed methodology for high-rise building design. **DOI: 10.1061/(ASCE)ST.1943-541X.0001164.** © *2014 American Society of Civil Engineers.*

Author keywords: Topology optimization; Linearized buckling; High-rise buildings.

Introduction

Topology optimization has been attracting increasing interest in the civil engineering industry, especially for the design of high-rise buildings and long-span structures. Several examples of applications of topology optimization for architectural design have been presented in Stromberg et al. (2012), Adams et al. (2012), and Martini (2011). In such examples, the optimization problem was formulated in terms of compliance minimization, which is a major parameter of structural efficiency. However, the high-rise building problem is by nature characterized by multiple objectives, and several aspects must be considered in the design beyond overall compliance of the structure, such as stability, natural frequencies, interstory drifts, etc.

An important issue emphasized throughout this work is the importance of stability and second-order effects. In high-rise design, the proportions of the building and the applied loads can tremendously affect the overall performance. In the detailed description of the John Hancock of Boston given next, it is shown that, when using common design loads with an $H/500$ drift criteria (H being the building height), the second-order effects can cause amplification of the forces up to 43%. The relationship between the amplification factor and the building width is described as follows: A.F. $= 1/\{1-[\gamma D/(wH/\Delta)]\}$, where γ = building density [typically 1.6 kN/m^3(10 pcf) for a steel building), D = building dimension (in meters), w = the wind pressure [typically 1 kPa (20 psf)], and H/Δ = design criteria utilized (typically $H/500$). Thus, A.F. $= 1/(1-0.001D)$. The values of the amplification factor for typical building widths are summarized in the Table 1. Notice that for typical building widths in the range of 30–60 m (100–200 ft), the force amplification is up to 25%, which is very significant in high-rise design, thus providing motivation for the studies presented in this work.

Many techniques have been developed for optimization of single objective problems. For example, Sigmund (2001), Bendsoe and Sigmund (2002), and Stromberg et al. (2012), among many others, focus on minimum compliance as the objective. Natural frequency and mass are the objective functions in studies by Diaz and Kikuchi (1992), Huang and Xie (2010), and Niu et al. (2008). Furthermore, Neves et al. (1995) tailor topology optimization design framework for stability problems, where the objective function is the critical buckling load. As for tip deflection as the objective function, the technique in Baker (1992) has been used for truss optimization, where the minimum volume subject to a target tip displacement is optimized.

In Stromberg et al. (2012), the focus was given to design the lateral bracing systems for high-rise buildings using compliance as the objective. This work aims to extend the previous methodology for other objective functions with particular attention to linearized buckling. Several examples are given to show the effectiveness of the methodology for the design of single-story and multistory portal frames. In addition, in Stromberg et al. (2012), the combination of continuum and discrete elements was used to overcome some of the shortcomings of using continuum elements only for a very sparse problem, such as the high-rise one. Here, this approach is retained; however, it has been extended to allow simultaneous sizing of the cross-sectional areas of the discrete members and optimization of the continuum elements. This extension is necessary because the assumption of constant stress used in Stromberg et al. (2012) does not hold for all objective functions (i.e., buckling).

There are alternatives for the design of tall buildings. Although core-megacolumn systems with outrigger and belt trusses are seen in some elements of modern design, this is not the case for all of today's high-rise designs. For example, braced diagrid structures (similar to those presented in this work) have been used recently (by the authors and by others) in the designs of proposals for the

[1]Graduate Student, Dept. of Civil Engineering, Univ. of Illinois at Urbana-Champaign, 205 N. Mathews Ave., Urbana, IL 61801. E-mail: lstromb2@illinois.edu

[2]Associate, Skidmore, Owings & Merrill, LLP, 224 S. Michigan Ave., Chicago, IL 60604. E-mail: alessandro.beghini@som.com

[3]Partner, Skidmore, Owings & Merrill, LLP, 224 S. Michigan Ave., Chicago, IL 60604. E-mail: william.baker@som.com

[4]Professor, Dept. of Civil Engineering, Univ. of Illinois at Urbana-Champaign, 205 N. Mathews Ave., Urbana, IL 61801 (corresponding author). E-mail: paulino@illinois.edu

Note. This manuscript was submitted on March 3, 2013; approved on August 6, 2014; published online on September 25, 2014. Discussion period open until February 25, 2015; separate discussions must be submitted for individual papers. This paper is part of the ***Journal of Structural Engineering***, © ASCE, ISSN 0733-9445/04014207(10)/$25.00.

Table 1. Amplification Factor for Second-Order Effects as a Function of the Building Proportions

D [m (ft)]	A.F.
23 (75)	1.08
30 (100)	1.11
60 (200)	1.25
90 (300)	1.43

San Francisco Transbay Transit Center, the Leadenhall Building (2014), Heron Tower (2011), Guangzhou International Finance Center (2010), Hearst Tower (2006), and even an earlier scheme of the upcoming Freedom Tower. Therefore, lateral bracing systems are the focus of this work.

The remainder of this paper is organized as follows. In the next section, previous investigations for buckling optimization are discussed and compared with the framework introduced here. Then, the importance of buckling in high-rise design is discussed in relation to actual buildings. The single-objective framework for continuum optimization is then introduced for buckling, and generalized for other objectives. The framework is also updated to include the cross-sectional areas of the discrete elements as design variables. A detailed sensitivity derivation is included for both the continuum and discrete elements. Numerical examples are given to demonstrate this framework for single-module frames to establish a benchmark and verify the authors' results. The framework is then applied to compare the objectives for practical bracing systems, and the paper concludes with some final remarks on the extensions of this work.

Literature Review

In the vast majority of papers on topology optimization, minimum compliance is used as the objective function. For the practicing engineer, other quantities, such as buckling, natural frequency, tip deflection, strength, interstory drift, cost, and combinations thereof, are of interest during the design of a structure. This section reviews current methods available in the literature, specifically for buckling optimization.

Typical topology optimization results often contain very slender members; therefore, the work by Neves et al. (1995) was one of the first in which a buckling load criterion was considered to address this issue. This was later expanded upon by Min and Kikuchi (1997), in which the homogenization method was used for the optimal reinforcement design of portal (single-story) frames under a buckling load. Similarly, the optimal design of plate reinforcements using a nonsmooth buckling load criterion was explored in the work by Folgado and Rodrigues (1998). Later, Rahmatalla and Swan (2003), Rahmatalla (2004), and Swan (2012) applied the use of buckling as an optimization criterion for the design of sparse, long-span bridges. Other contributors to the continuum topology optimization problem with buckling as an objective are Zyczkowski and Gajewski (1988), Sekimoto and Noguchi (2001), and Bendsoe and Sigmund (2002). Extensions for buckling problems in materials can be found in the paper by Neves et al. (2002). To make design problems more realistic, geometric nonlinearities were incorporated in the stability problem for *perfect* and *imperfect* structures in Kemmler et al. (2005) by directly determining the critical load factor and including it as an inequality constraint.

It should be noted that many numerical issues are encountered in the buckling optimization problem. One of the main issues associated with topology optimization for buckling is the presence of localized eigenmodes. To eliminate this effect, many techniques artificially remove *void* elements from the optimization problem; however, this may produce erroneous solutions because, when an element is removed, it cannot reenter the optimization problem (Pedersen 2000). An alternative methodology to eliminate localized eigenmodes in low-density areas for cases in which the problem is not formulated as reinforcement of an existing structure is presented in Pedersen (2000). Other numerical issues include the case of multiple eigenvalues, which are typically present in symmetric structures, and nonsmoothness of the eigenvalues (Olhoff and Rasmussen 1977). For a review of multiple eigenvalues in structural optimization problems and how to treat them, the reader can refer to the work by Seyranian et al. (1994). The implementation proposed here includes an adapted version of the method suggested by Olhoff and Du (2012) to stabilize the structure and eliminate problems with local effects. Furthermore, in this work, the authors assume simple (nonrepeated) eigenvalues, although differentiability issues associated with repeated eigenvalues might be avoided by reducing the design space in accordance with structural symmetry (Kosaka and Swan 1999).

Buckling and Second-Order Effects in High-Rise Building Design

In high-rise building design, multiple structural objectives can be considered—mainly, overall drift, compliance, period, and buckling. Each objective relates to a different aspect of the design, but they all ultimately affect the topological layout of the structural system and the sizing of the members.

Building drift (measured by the ratio of the displacement at the top of the building to the height of the building, H) under lateral loads has traditionally been used as a good indicator of adequate stiffness. A building with drift less than $H/500$ would be deemed adequate, in terms of having a properly sized lateral structural system. Recently, compliance, which measures the work done by the external applied loads on the building, has been considered to maximize the overall stiffness of the lateral system. Compliance is a global indicator of stiffness because it considers the displacements at each point of load application in the calculations, whereas building drift is more of a local measure because it considers only the tip displacements. Minimizing the building period is another important objective, because a shorter period typically means better overall wind performance. Buckling and second-order effects in general are another aspect which must be addressed to ensure the global stability of the structure and to include P-delta effects in member design.

To better understand the importance of buckling and second-order effects in high-rise building design, the authors outline a simple example inspired by the work of LeMessurier (1976, 1977). Such work was developed as a result of the issues and investigations associated with the construction of the John Hancock Tower in Boston in the mid 1970s. Consider the structure in Fig. 1(a), which conceptually represents a high-rise building under gravity loads, P, with lateral load system represented by the linear spring stiffness, k. For a small horizontal (virtual) displacement, δ, the moment equilibrium at the base reads $P\delta = k\delta H$, which is equivalent to the eigenvalue problem $(kH - P)\delta = 0$. Therefore, the critical buckling load for the building is $P_{cr} = kH$. To define the stiffness, k, consider Fig. 1(b), where the lateral loads on the structure are represented by the force, V. Using the notation in the figure, $V = k\Delta_0$. Here, Δ_0 represents the building tip displacement without considering second-order effects, and Δ_0/H is the first-order building drift. The critical buckling load for the building now reads $P_{cr} = VH/\Delta_0$. Note that using the traditional design approach, the structure would be designed to ensure $\Delta_0/H < 1/500$. Now superimpose the effects of gravity and lateral loads, as shown in Fig. 1(c). The moment equilibrium with respect to the base reads $k\Delta H - P\Delta - VH = 0$, or

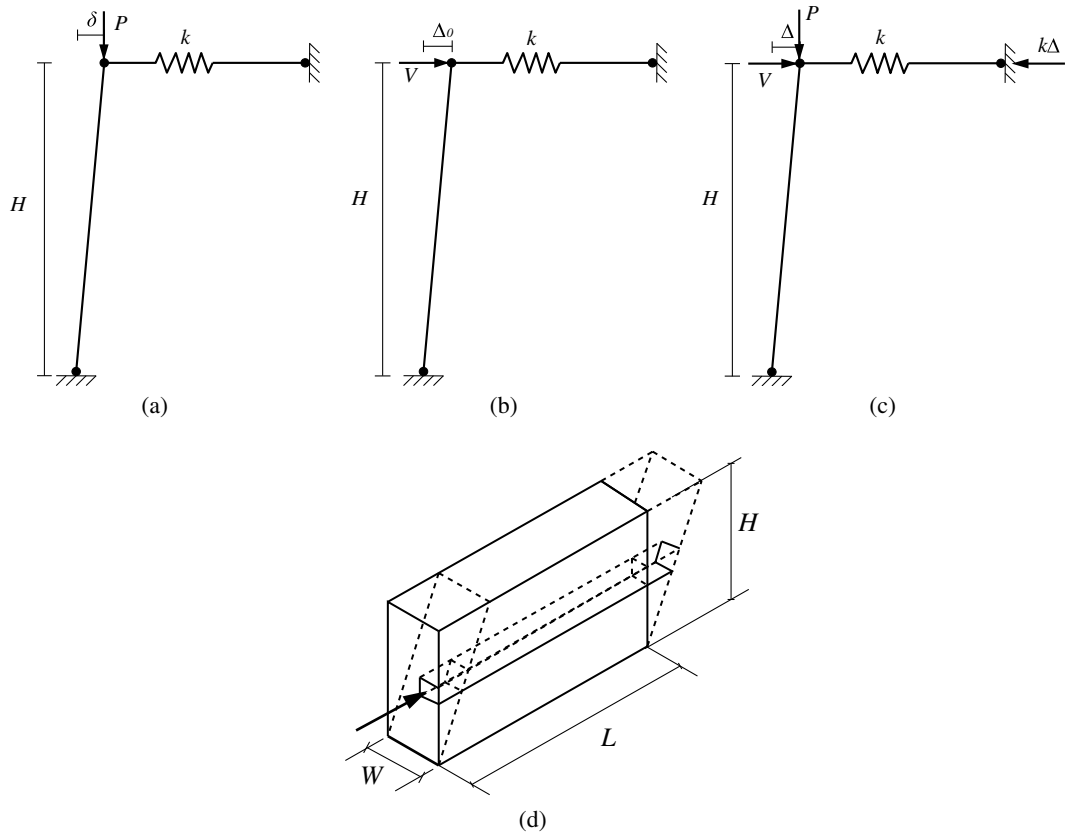

Fig. 1. Second-order effects in high-rise buildings: (a) gravity loads; (b) lateral loads; (c) combined gravity and lateral loads; (d) second-order effects in a rectangular building

$$\Delta = \frac{VH}{kH - P} = \frac{P_{cr}\Delta_0}{P_{cr} - P} \tag{1}$$

where Δ = horizontal displacements accounting for second-order effects. Eq. (1) can be rewritten as follows:

$$\frac{\Delta}{\Delta_0} = \frac{1}{1 - P/P_{cr}} = \text{A.F.} \tag{2}$$

The aforementioned amplification factor (A.F.) indicates the amplification of the first-order drift due to the second-order effects caused by the gravity loads in the system, and it has been incorporated in design codes since the 1970 s. To quantify such effect on a high-rise building, consider the example in Fig. 1(d), which is similar to the example described by LeMessurier (1977). The building considered has a rectangular plan with $W = 30$ m (100 ft), $L = 90$ m (300 ft), and $H = 60$ m (200 ft). In addition, the authors assume a wind pressure of 1 kPa (20 psf) acting on the narrow face of the building and a building density of 1.6 kN/m^3 (10 pcf) (typical for a steel building). Considering the prismatic element through the building in Fig. 1(d) with a base of 1 m^2 (1 ft^2) and length L, and assuming the drift criteria $\Delta_0/H = 1/500$ gives $P_{cr} = VH/\Delta_0 = 1$ kPa (20 psf) $\cdot$ 500 $\cdot$ 1 m^2 (1 ft^2) = 500 kN(10,000 lbs). The gravity load of the prismatic element would be $P = 1.6$ kN/m 3 (10 pcf) $\cdot$ 90 m (300 ft) $\cdot$ 1 m^2 (1 ft^2) = 144 kN (3,000 lbs). The amplification factor on the second-order effects for the narrow face would be A.F. $= 1/(1 - 144/500) = 1.43$. Similarly, the amplification factor for the wider face would be A.F. $= 1/(1 - 48/500) = 1.1$, which is much less. Therefore, by using only the first-order drift as a design criterion in both directions, the lateral system would be significantly undersized in the long direction because the wind load on the narrow face causes small forces, but the second-order amplification effects would be very large. Investigations on the Hancock Tower in Boston triggered by other issues unearthed this stability problem, which was solved by strengthening the core elements. An extreme design case of a condition with small lateral forces would be the situation of a very large (in plan) warehouse building in a very low seismic area. Such building would have very large gravity loads applied, and because expansion joints are required every 90 m (300 ft) or so, it is conceivable to have a structure in the middle of the warehouse complex which is shielded on all sides and therefore not requiring, in principle, any lateral system. In such a situation, buckling considerations and second-order effects would control the design. Notice that the modern codes acknowledge such possibilities, and a minimum (notional) lateral load should always be factored in the design.

The aforementioned examples emphasize three key aspects: (1) in a certain class of high-rise buildings, buckling considerations control the design over drift considerations; (2) second-order effects can cause significant force amplifications; and (3) a simple superposition of effects (gravity loads and lateral loads) would not capture the second-order effects. Therefore, a methodology to maximize the buckling load would be very beneficial to structural engineers; such methodology is the main focus of this paper.

Linearized Buckling Framework

The single-objective framework for linearized buckling is discussed here. Buckling is used as an example of another objective relevant to structural engineers beyond compliance, although similar formulations for other structural objectives could be introduced.

The sensitivity analysis is described next for a generic objective, and buckling is used as an example.

Problem Statement and Formulation

The generalized eigenvalue problem for linearized buckling can be stated as follows:

$$[\mathbf{K}(\mathbf{d}) + P_{\text{cr}}\mathbf{K}_{\mathbf{g}}(\mathbf{u},\mathbf{d})]\phi = 0 \tag{3}$$

or

$$[\mathbf{K}_{\mathbf{g}}(\mathbf{u},\mathbf{d}) + \lambda\mathbf{K}(\mathbf{d})]\phi = 0 \tag{4}$$

where $\mathbf{K}(\mathbf{d})$ = stiffness matrix as a function of the design variables, $\mathbf{d}$, $\mathbf{u}$ = vector of nodal displacements, P_{cr} = critical buckling load, $\mathbf{K}_{\mathbf{g}}$ = geometric stiffness matrix, $\lambda = 1/P_{\text{cr}}$ is the eigenvalue, and ϕ = its associated eigenvector. The authors note that the solid isotropic material penalization (SIMP) model (Bendsoe 1989; Rozvany et al. 1992; Bendsoe and Sigmund 1999) is used in the computation of the stiffness matrices to gear the optimization toward a 0–1 solution by penalizing intermediate (gray) design variables

$$E(\mathbf{d}) = E_0\mathbf{d}^p \tag{5}$$

where $E(\mathbf{d})$ = stiffness of design variable $\mathbf{d}$, p = penalization with $p \geq 1$, and E_0 = Young's modulus of solid material. The geometric stiffness matrix, $\mathbf{K}_{\mathbf{g}}$, is given by

$$\mathbf{K}_{\mathbf{g}} = \int \mathbf{G}^T \begin{bmatrix} \mathbf{s} & \mathbf{0} & \mathbf{0} \\ \mathbf{0} & \mathbf{s} & \mathbf{0} \\ \mathbf{0} & \mathbf{0} & \mathbf{s} \end{bmatrix} \mathbf{G}dV \tag{6}$$

where $\mathbf{s}$ = initial stress tensor:

$$\mathbf{s} = \begin{bmatrix} \sigma_{x0} & \tau_{xy0} & \tau_{zx0} \\ \tau_{xy0} & \sigma_{y0} & \tau_{yz0} \\ \tau_{zx0} & \tau_{yz0} & \sigma_{z0} \end{bmatrix} \tag{7}$$

and the terms in $\mathbf{G}$ in Eq. (6) are obtained from the differentiation of the shape functions in $\mathbf{N}$ (Cook et al. 2001). The objective, f, is to maximize the minimum critical buckling load in terms of $\mathbf{d}$ as follows:

$$\min_{\mathbf{d},\mathbf{u}(\mathbf{d})} f[\mathbf{d},\mathbf{u}(\mathbf{d})] = \min\left[\max_{i=1\ldots N\text{Dof}}(\lambda_i)\right] = \min\left(\frac{1}{P_{\text{cr}}}\right)$$
$$= \min\left[\max\left(-\frac{\phi^T\mathbf{K}_{\mathbf{g}}\phi}{\phi^T\mathbf{K}\phi}\right)\right]$$

Thus, the problem statement can be written using a nested formulation (Christensen and Klarbring 2008) as

$$\begin{aligned} \min_{\mathbf{d},\mathbf{u}(\mathbf{d})} \quad & f[\mathbf{d},\mathbf{u}(\mathbf{d})] = \max_i \lambda_i \\ \text{s.t.} \quad & g_1[\mathbf{d},\mathbf{u}(\mathbf{d})] = V(\mathbf{d}) - \bar{V} \\ & 0 \leq d_i \leq 1 \end{aligned} \tag{8}$$

where $\mathbf{u}(\mathbf{d})$ is defined implicitly through the equilibrium equation, $\mathbf{K}(\mathbf{d})\mathbf{u}(\mathbf{d}) = \mathbf{p}$, where $\mathbf{p}$ = vector of applied nodal loads; g_1 = constraint on the volume of material; $\bar{V}$ = the allowable total volume; and the ith eigenvalue is

$$\lambda_i = -\frac{\phi_i^T\mathbf{K}_{\mathbf{g}}\phi_i}{\phi_i^T\mathbf{K}\phi_i} \tag{9}$$

Derivation of Sensitivities

To use a gradient-based update scheme for the optimization, the design gradient of the objective function must be computed. Next, the expression for the gradient is derived for a general objective function, with linearized buckling given as an example.

Using a nested formulation (Christensen and Klarbring 2008), the general objective function is $F_r(\mathbf{d}) = F[\mathbf{d},\mathbf{u}(\mathbf{d})]$, in which $\mathbf{u}$ is implicitly defined as a solution to the equilibrium equation $\mathbf{K}(\mathbf{d})\mathbf{u} = \mathbf{p}$, where $\mathbf{u}$ = a vector containing the structural response, which is displacement in this case; $\mathbf{K}(\mathbf{d})$ = stiffness matrix as a function of the design variable, $\mathbf{d}$; and $\mathbf{p}$ = applied external forces. The authors note that in this case, the design variable were selected as the element densities with $d = 0$ signifying a void and $d = 1$ representing solid material. The sensitivity of the objective function with respect to the design variable, d_i, is thus given using a chain rule as follows:

$$\frac{\partial F_r}{\partial d_i} = \frac{\partial F}{\partial d_i}[\mathbf{d},\mathbf{u}(\mathbf{d})] + \sum_{j=1}^{n}\frac{\partial F}{\partial u_j}[\mathbf{d},\mathbf{u}(\mathbf{d})]\frac{\partial u_j}{\partial d_i}(\mathbf{d})$$
$$= \frac{\partial F}{\partial d_i}[\mathbf{d},\mathbf{u}(\mathbf{d})] + \{\nabla_{\mathbf{u}}F[\mathbf{d},\mathbf{u}(\mathbf{d})]\}^T\frac{\partial \mathbf{u}(\mathbf{d})}{\partial d_i}(\mathbf{d}) \tag{10}$$

where u_j = jth displacement as a function of the i design variable, with n being the total number of degrees of freedom. To obtain an explicit expression for $[\partial\mathbf{u}(\mathbf{d})/\partial d_i]$, the equilibrium expression is differentiated with respect to d_i

$$\frac{\partial \mathbf{K}(\mathbf{d})}{\partial d_i}\mathbf{u}(\mathbf{d}) + \mathbf{K}(\mathbf{d})\frac{\partial \mathbf{u}(\mathbf{d})}{\partial d_i} = \frac{\partial \mathbf{p}(\mathbf{d})}{\partial d_i} \tag{11}$$

$$\frac{\partial \mathbf{u}(\mathbf{d})}{\partial d_i} = \mathbf{K}^{-1}(\mathbf{d})\left[\frac{\partial \mathbf{p}(\mathbf{d})}{\partial d_i} - \frac{\partial \mathbf{K}(\mathbf{d})}{\partial d_i}\mathbf{u}(\mathbf{d})\right] \tag{12}$$

Substituting Eq. (12) into Eq. (10), the sensitivity of the objective function can then be written as

$$\frac{\partial F_r}{\partial d_i} = \frac{\partial F}{\partial d_i}[\mathbf{d},\mathbf{u}(\mathbf{d})]$$
$$+ \{\mathbf{K}^{-\mathbf{T}}\nabla_{\mathbf{u}}F[\mathbf{d},\mathbf{u}(\mathbf{d})]\}^T\left[\frac{\partial \mathbf{p}(\mathbf{d})}{\partial d_i} - \frac{\partial \mathbf{K}(\mathbf{d})}{\partial d_i}\mathbf{u}(\mathbf{d})\right] \tag{13}$$

The adjoint displacement, $\mathbf{u}_{\mathbf{a}}$, can be defined as follows:

$$\mathbf{u}_{\mathbf{a}} = \{\mathbf{K}^{-\mathbf{T}}\nabla_{\mathbf{u}}F[\mathbf{d},\mathbf{u}(\mathbf{d})]\}^T \tag{14}$$

or

$$\mathbf{K}(\mathbf{d})\mathbf{u}_{\mathbf{a}} = \nabla F[\mathbf{d},\mathbf{u}(\mathbf{d})] \tag{15}$$

Thus, in general, for *any* objective function, the sensitivities of the design variables can be written as follows:

$$\frac{\partial F_r}{\partial d_i} = \frac{\partial F}{\partial d_i}[\mathbf{d},\mathbf{u}(\mathbf{d})] + \mathbf{u}_{\mathbf{a}}\left[\frac{\partial \mathbf{p}(\mathbf{d})}{\partial d_i} - \frac{\partial \mathbf{K}(\mathbf{d})}{\partial d_i}\mathbf{u}(\mathbf{d})\right] \tag{16}$$

As an example, for the linearized buckling problem, the objective function can be written as follows:

$$F[\mathbf{d},\mathbf{u}(\mathbf{d})] = \frac{1}{P_{\text{cr}}} = \lambda_{\max} \tag{17}$$

The generalized eigenvalue problem given in Eq. (3)

$$\phi^T\mathbf{K}_{\mathbf{g}}(\mathbf{u},\mathbf{d})\phi = -\lambda_{\max}\phi^T\mathbf{K}(\mathbf{d})\phi \tag{18}$$

can be substituted into Eq. (17) to provide

$$F[\mathbf{d}, \mathbf{u}(\mathbf{d})] = \frac{1}{P_{\text{cr}}} = \lambda_{\max} = -\frac{\phi^T \mathbf{K_g} \phi}{\phi^T \mathbf{K} \phi} \tag{19}$$

Differentiating Eq. (18), one obtains the following relationship:

$$\phi^T \frac{\partial \mathbf{K_g}(\mathbf{u}, \mathbf{d})}{\partial d_i} \phi + \lambda_{\max} \phi^T \frac{\partial \mathbf{K}(\mathbf{d})}{\partial d_i} \phi - \frac{\partial \lambda_{\max}}{\partial d_i} \phi^T \mathbf{K}(\mathbf{d}) \phi = 0 \tag{20}$$

Rearranging terms and normalizing the stiffness matrix, such that $\phi^T \mathbf{K}(\mathbf{d}) \phi = 1$, one obtains

$$\begin{aligned} \frac{\partial \lambda_{\max}}{\partial d_i} &= \left[\phi^T \frac{\partial \mathbf{K_g}(\mathbf{u}, \mathbf{d})}{\partial d_i} \phi + \lambda_{\max} \phi^T \frac{\partial \mathbf{K}(\mathbf{d})}{\partial d_i} \phi \right] \\ &= \phi^T \left[\frac{\partial \mathbf{K_g}(\mathbf{u}, \mathbf{d})}{\partial d_i} + \frac{1}{P_{cr}} \frac{\partial \mathbf{K}(\mathbf{d})}{\partial d_i} \right] \phi \end{aligned} \tag{21}$$

The adjoint problem for buckling as an objective function thus becomes

$$\mathbf{K}(\mathbf{d}) \mathbf{u_a} = \nabla_{\mathbf{u}} F[\mathbf{d}, \mathbf{u}(\mathbf{d})] = \frac{\partial F[\mathbf{d}, \mathbf{u}(\mathbf{d})]}{\partial \mathbf{u}} = -\phi^T \frac{\partial \mathbf{K_g}[\mathbf{d}, \mathbf{u}(\mathbf{d})]}{\partial \mathbf{u}} \phi \tag{22}$$

where

$$\frac{\partial \mathbf{K_g}[\mathbf{d}, \mathbf{u}(\mathbf{d})]}{\partial u_i} = \begin{bmatrix} \frac{\partial \mathbf{s}}{\partial u_i} & \mathbf{0} \\ \mathbf{0} & \frac{\partial \mathbf{s}}{\partial u_i} \end{bmatrix} \tag{23}$$

Assuming plane stress, the authors obtain

$$\frac{\partial \mathbf{s}}{\partial u_i} = \frac{E_0}{1 - \nu^2} \begin{bmatrix} \frac{\partial N_i}{\partial x} & \left(\frac{1-\nu}{2}\right) \frac{\partial N_i}{\partial y} \\ \left(\frac{1-\nu}{2}\right) \frac{\partial N_i}{\partial y} & \nu \frac{\partial N_i}{\partial x} \end{bmatrix} \tag{24}$$

Finally, the authors arrive at the following expression for the sensitivities of the design variables with respect to the critical buckling load:

$$\frac{\partial F_r}{\partial d_i} = \phi^T \left[\frac{\partial \mathbf{K_g}(\mathbf{d})}{\partial d_i} + \frac{1}{P_{\text{cr}}} \frac{\partial \mathbf{K}(\mathbf{d})}{\partial d_i} \right] \phi - \mathbf{u_a} \frac{\partial \mathbf{K}(\mathbf{d})}{\partial d_i} \mathbf{u}(\mathbf{d}) \tag{25}$$

For other objective functions, a procedure can be followed similar to that of Eqs. (17)–(25).

Sensitivities of the Discrete Elements

The combination of discrete and continuum elements to overcome the shortcomings associated with the accumulation of material observed in the analysis with only continuum elements was introduced in Stromberg et al. (2012). Here, the same approach is utilized, but the areas of the discrete elements are included in the optimization problem. To this end, the sensitivities are calculated starting from Eq. (16), which provides a general expression for any objective. In this case, the authors select d_i as the cross-sectional area of the ith discrete member. For the case of compliance minimization, $\mathbf{p}$ is independent of $\mathbf{d}$ and $\nabla_{\mathbf{u}} F[\mathbf{d}, \mathbf{u}(\mathbf{d})] = \mathbf{p}$ so $\mathbf{u_a} = \mathbf{u}(\mathbf{d})$, simplifying the sensitivity expression to

$$\frac{\partial F_r}{\partial d_i} = -\mathbf{u}(\mathbf{d})^T \frac{\partial \mathbf{K}(\mathbf{d})}{\partial d_i} \mathbf{u}(\mathbf{d}) \tag{26}$$

For buckling optimization, Eq. (25) remains the same as before, but for the discrete element, the contribution from the axial stress is

$$\frac{\partial \mathbf{s}}{\partial u_i} = \frac{E_0}{L} \tag{27}$$

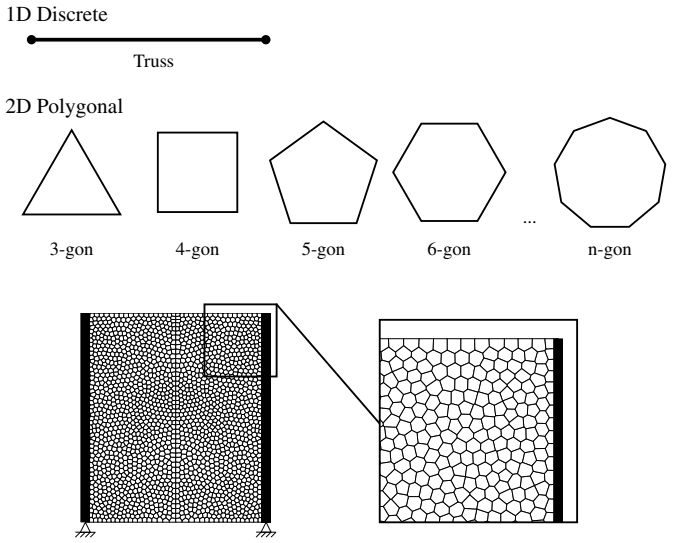

Fig. 2. Elements investigated in this research and discretization of design domain using these elements

Computational Framework

The computational framework developed in this research was based on a combination of polygonal finite elements (Talischi et al. 2012a, b) and discrete (truss) finite elements. In Fig. 2, the types of elements used in this study are shown, which include one-dimensional (1D) discrete truss elements and two-dimensional (2D) polygonal elements, ranging from 3-gons to n-gons. Two discrete truss elements were used to model the columns to eliminate several issues encountered with the high-rise problem, such as unrealistic flexural stiffness associated with continuum elements used to model the columns, inability to identify the resulting locations of the connections and working points, formation of incomplete bracing systems, etc. These issues are described in detail in Stromberg et al. (2012).

The polygonal finite elements were used in this framework to model the continuum subdomain, in which the bracing system could form, as shown in Fig. 2. The polygonal elements were selected due to their ability to naturally eliminate unstable checkerboard patterns and one-node connections, often present with traditional triangular or quadrilateral finite-element meshes, caused by their artificial stiffness in the finite-element approximation (Talischi et al. 2010). Additionally, it has been shown in Talischi et al. (2010) that the choice of polygonal finite elements allows unstructured meshes to be easily generated using Voronoi tessellations, which can also be used to eliminate bias in the orientation of the resulting *members*, as typical triangles and quadrilaterals often constrain these orientations with the geometry of the mesh, often resulting in mesh-dependent suboptimal designs.

Numerical Examples

As described extensively in Stromberg et al. (2012), in the high-rise problem using only continuum elements, material tends to concentrate at the ends of the design domain to resist the overturning moment, generating thick bands of material representing the columns. Such bands introduce unrealistic bending stiffness and require the use of discrete elements to accurately capture the behavior of the structure. In addition, discrete elements have the advantage of making the working points easy to identify. On the other hand, the disadvantage of using discrete elements is that the number of members and the connectivity must be known a priori to carry out the

optimization, unless other techniques, such as ground structures [see Chapter 4 of Bendsoe and Sigmund (2002) and Chapter 5 of Christensen and Klarbring (2008)], are used. The continuum approach has the advantage that the layout of the structure is free to form within the whole domain. The discrete/continuum framework here is the best compromise for the high-rise problem because the discrete members are located where the columns are typically located (at the corners on the perimeter of the building), whereas the continuum is available to form the optimal layout of the diagonals.

As an extension to the methodology introduced in Stromberg et al. (2012), the cross-sectional areas of the discrete members can be incorporated in the optimization problem, in addition to the element densities of the continuum elements, to further streamline the design process. In this case, the method of moving asymptotes (Svanberg 1987) is selected as the optimization engine due to its flexibility in incorporating several optimization objectives and constraints.

To establish a benchmark for the optimization solution, several single-objective (i.e., compliance, buckling) studies are conducted next, first using discrete elements only, and then using the proposed integrated discrete/continuum framework.

Discrete Studies: Comparison of Objective Functions

Minimum Compliance

Revisiting the one-story braced frame from Stromberg et al. (2012), Fig. 3(a) shows the problem statement for minimum compliance as the objective function, in which the total volume is $\bar{V} = 1$ m^3; the height, $H = 48$ m; the width; $2B = 41.5$ m; and the applied lateral loads, $P_{\text{total}} = 2$ MN (1 MN applied at each tip). The problem statement is given, using a nested formulation (Christensen and Klarbring 2008) as described previously, as follows:

$$\begin{aligned} \min_{\mathbf{d},\mathbf{u}} \quad & f(\mathbf{d},\mathbf{u}) = \mathbf{u}^T\mathbf{K}(\mathbf{d})\mathbf{u} \\ \text{s.t.} \quad & g_1[\mathbf{d},\mathbf{u}(\mathbf{d})] = V(\mathbf{d}) - \bar{V} \\ & 0 \le d_i \le 1 \end{aligned} \tag{28}$$

In the following discrete examples, the design variables, $\mathbf{d}$, are selected as the cross-sectional areas of the members. The numerical optimization is then conducted using MATLAB's fmincon for the simple purely discrete benchmark study, which finds the minimum of a constrained multivariable function.

On the right of Fig. 3(a), the total minimum compliance, c, using the cross-sectional areas as the design variables for various elevations of the bracing point ratio, z/H, is shown. At the optimum, $z = 36$ m, $c = 1{,}538$ kN-m, and the corresponding optimal cross-sectional areas are reported in Table 2. The authors note here that the stress is constant within all members, $\sigma = 555$ MPa. Analyzing the optimal structure for the gravity load case shown in Fig. 3(b), the critical buckling load factor computed using these cross-sectional areas is $P_{cr} = 104.1$.

Maximization of Critical Buckling Load

For the same problem given in the previous section, the critical buckling load is now maximized for the gravity load case shown in Fig. 3(b) using the problem statement given in Fig. 3(b) and Eq. (8). Fig. 3(b) shows a similar trend in regards to the behavior of the compliance problem, and remarkably, the optimal bracing point occurs at the same location: $z = 36$ m. This can be explained

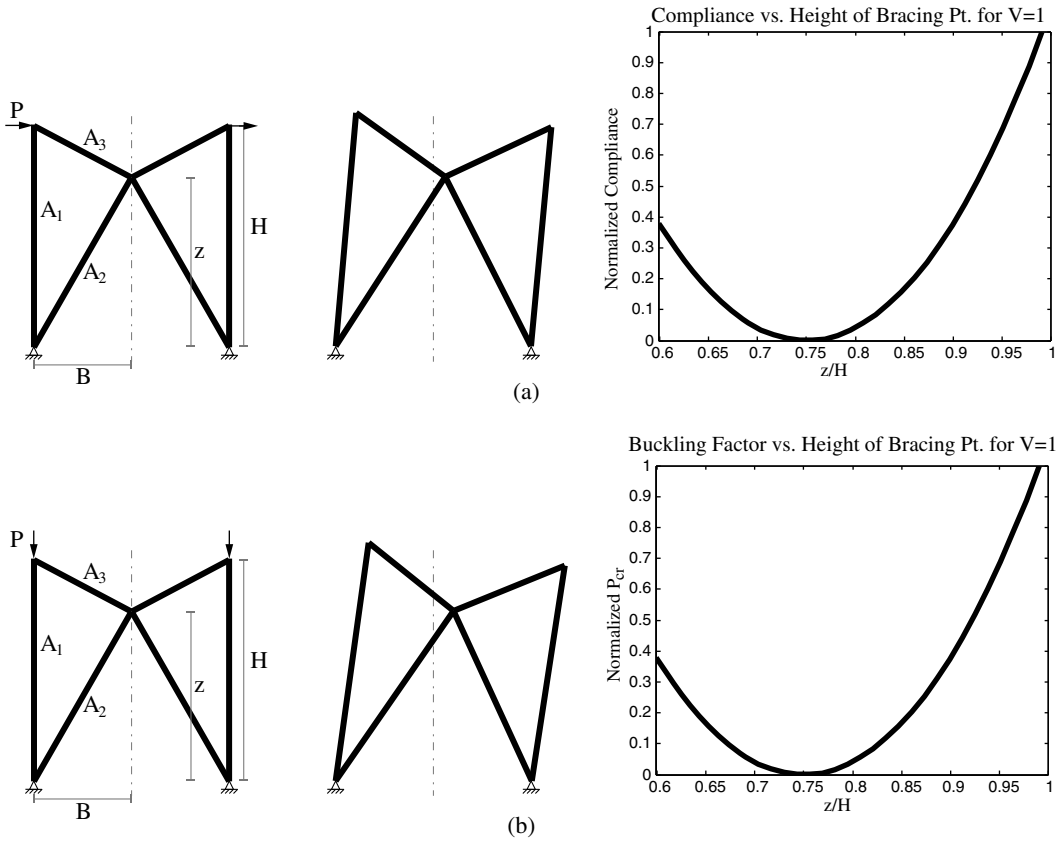

Fig. 3. Problem statement, deflected or mode shape, and convergence of the following optimization problems to find the location of the bracing point ratio, z/H, and cross-sectional areas, A_i, for a fixed volume, $\bar{V} = 1$ m^3 with $P = 1$ MN: (a) minimum compliance of the wind load case; (b) maximization of minimum critical buckling load for gravity load case

J. Struct. Eng., 2015, 141(8): -1--1

Table 2. Comparison of Objectives and Cross-Sectional Areas for the Problems in Fig. 3

Variable	Objective	
	Compliance	Buckling
z (m)	36	36
c (kN-m)	1,538	1,593
P_{cr}	104.1	111.5
A_1 (m^2)	0.0021	0.0030
A_2 (m^2)	0.0072	0.0064
A_3 (m^2)	0.0042	0.0037

by the similarities between the critical buckling mode of the gravity load case and the deflected shape of the wind load case. At the optimum, the critical buckling load factor, $P_{cr} = 111.5$, is higher than that of the minimum compliance problem, as expected. A summary of the corresponding cross-sectional areas is given in Table 2. The authors note that if the compliance is computed for the lateral load case of Fig. 3(a) using the optimal cross-sectional areas of the buckling problem, $c = 1{,}593$ kN-m is obtained—slightly higher (worse) than that with minimum compliance as the objective.

Note that the buckled shape in Fig. 3(b) resembles the deformed wind shape because truss elements were used. If beam elements were used, other buckled shapes with a lower eigenvalue could control the design. However, columns are typically designed to resist buckling, and here the focus is on a system level buckling neglecting local phenomena.

The results presented in Fig. 3(a) follow the analytical approach described in Stromberg et al. (2012) for the case of lateral loads. In compliance/tip deflection minimization, each cross-sectional area is sized proportionally to the strain energy in each member. In the buckling optimization illustrated in Fig. 3(b), the stiffness of the lateral systems is still maximized [similarly to the problem in Fig. 3(a)], but the strain energy in the columns is higher due to the vertical loads, thus some material is shed from the diagonals to the columns as described in Table 2.

Combined Discrete/Continuum Element Studies

The cases analyzed in the previous section are now solved using a discretization of 5,000 polygonal finite elements (Talischi et al. 2012a, b) for the continuum (braces) and two truss elements for the columns with the method of moving asymptotes (Svanberg 1987) for the optimization, as described previously. The thickness of the continuum is selected as $t = 0.002$ m. The topology optimization is run until convergence for $p = 1$ to determine the optimal member sizes so as not to bias the stiffness of the discrete elements based on their cross-sectional areas with the penalization of the stiffness in the continuum formulation. The resulting sizes are then used with continuation for $p = 1$ to 4 to determine the final topology of the *diagonal* members. For the minimum compliance of the lateral load case [Fig. 4(a)], $c = 1{,}586$ kN-m, $A = 0.0020$ m^2, and $P_{cr} = 75.9$. The contribution from the continuum is $c = 1{,}338$ kN-m and $c = 248$ kN-m from the discrete elements.

For the minimum compliance problem, it has been shown that the optimal solution is a fully stressed design. Thus, for comparison purposes, the authors analyze the stress in each of the members. For the columns, the stress can be computed as $\sigma_{col} = P_{col}/A_{col} = 513$ MPa. However, because the continuum *members* are

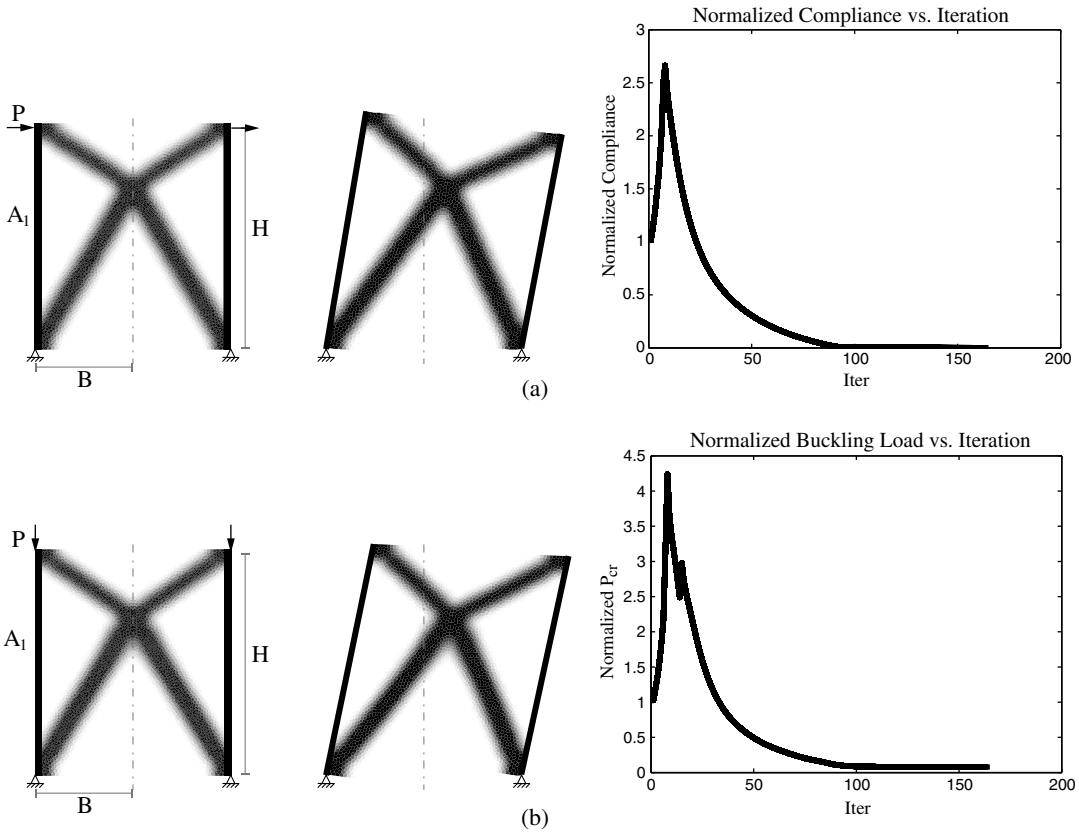

Fig. 4. Problem statement for the discrete/continuum implementation to find optimal geometry and cross-sectional area with $\bar{V} = 1$ m^3: (a) minimum compliance problem; (b) maximization of critical buckling mode

not as clearly defined as a truss is, the following equivalent quantity can be used:

$$\sigma_{\text{cont}} = \left[E\frac{c_{\text{continuum}}}{V_{\text{continuum}}}\right]^{1/2} = \left[\frac{(200{,}000\ \text{MPa})(1.338\ \text{MN-m})}{0.81\ \text{m}^3}\right]^{1/2} = 575\ \text{MPa} \tag{29}$$

where $c_{\text{continuum}}$ represents the contribution of the continuum elements to the overall compliance of the system. Comparing the stress in the columns with that in the braces, it can be seen that the values are roughly constant, thus showing that the solution is a fully stressed design.

It should be noted that, for the buckling problem, several issues are encountered in regards to localized buckling modes. To eliminate these modes, the geometric stiffness matrix, $\mathbf{K_g}$, can be computed using modified element densities, where the geometric stiffness is modified for element densities less than 10%, as suggested by Olhoff and Du (2012), following the equation below:

$$d = \begin{cases} d^6 & \text{for } 0 < d < 0.1 \\ d^p & \text{for } 0.1 \le d \le 1 \end{cases} \tag{30}$$

with $p = 6$ for the SIMP penalization parameter on the geometric stiffness given in Eq. (5).

In addition to the presence of localized modes, the occurrence of mode switching is quite common in topology optimization problems of a dynamic nature (see Fig. 5, for example) (Olhoff and Du 2012). To avoid this issue, in the proposed framework, the first mode (i.e., the one that is to be optimized) is selected from the first 10 eigenmodes based on an overall system (sidesway) buckled shape. At each subsequent iteration, the new eigenmodes are normalized and compared against the previous buckling mode, and the mode in which the norm of the difference is nearly zero is selected as the new mode to be optimized. This ensured that the topology optimization was performed for a global (sidesway) buckling mode throughout.

If the same problem is analyzed with the objective of maximizing the critical buckling factor, the final optimal geometry gives

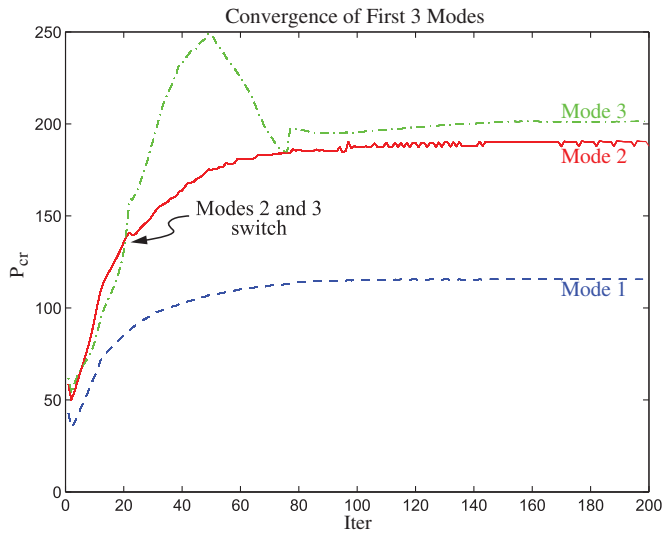

Fig. 5. Example of mode switching (common in dynamic optimization problems)

$P_{\text{cr}} = 111.5$, and the cross-sectional area of the columns is $A = 0.0030\ \text{m}^2$, which matches exactly with the discrete study given earlier. If this structure is then analyzed for compliance, the geometry produces $c = 1{,}613$ kN-m. The authors also note that, for the case in which the objective is to maximize the minimum critical buckling load, the assumption of constant stress does not hold.

From these examples, one can conclude that if a structure is optimized for compliance using the lateral load case, the final geometry (topology) will also be optimal for maximization of the critical buckling load; however, the column sizes will be different. Thus, from the compliance optimization, the optimal topology of the structure can be determined, which can then be sized for buckling using energy methods (Baker 1992; Stromberg et al. 2012).

Optimal Bracing Systems: Six-Story Building

The six-module bracing study originally presented in Stromberg et al. (2012) as the prototypical high-rise building problem is revisited here using the proposed framework. The overall dimensions of the structure are $H = 288$ m by $2B = 41.5$ m by $t = 0.036$ m, with an applied loading of $P = 2{,}000$ kN at each mega-story and a minimum member size of $r_{\text{min}} = 3$. The allowable volume of material is constrained to $\bar{V} = 240\ \text{m}^3$, and the material is assumed to be steel ($E = 200$ GPa). This example is analyzed for the cases of single-objective optimization using compliance and buckling, and for the combination of the two. The problem consists of a six-module portal frame with six discrete (truss) elements equally spaced along the height. The authors note that the discrete elements could alternatively use beam finite elements instead of trusses; however, this would only increase the computational time without adding significant information to the problem because it would only enable the column buckling to be captured, which is typically not a concern after proper structural sizing.

Discrete Study to Benchmark Objectives

Fig. 6(a) shows the results for the optimal geometry using discrete members only. As shown in the previous section, the compliance of the wind load case and the buckling of the gravity load case result in the same optimal geometry in terms of the frame layout, but different cross-sectional areas of the members (Table 3). Thus, the initial topology of the structure could be determined using compliance optimization of the wind load case, where the members are sized later in the process to incorporate buckling effects due to the gravity loading.

Combined Discrete/Continuum Approach for Minimum Compliance

Next, in Fig. 6(b), the results are shown using the discrete/continuum implementation proposed here; the associated column sizes are given in Table 3. These results confirm those of Fig. 29 in Stromberg et al. (2012) when the cross-sectional areas are added to the optimization problem. Moreover, the resulting column sizes are very close to the case of constant stress, as expected.

Combined Discrete/Continuum Approach for Maximization of Critical Buckling Load

When these applied loads are inverted from horizontal (lateral wind load) to vertical (gravity load), the results of Fig. 6(c) are produced with the associated optimal member sizes given in Table 3. Fig. 6(d) shows the corresponding final critical buckling load. The authors note here that the buckling objective function also takes

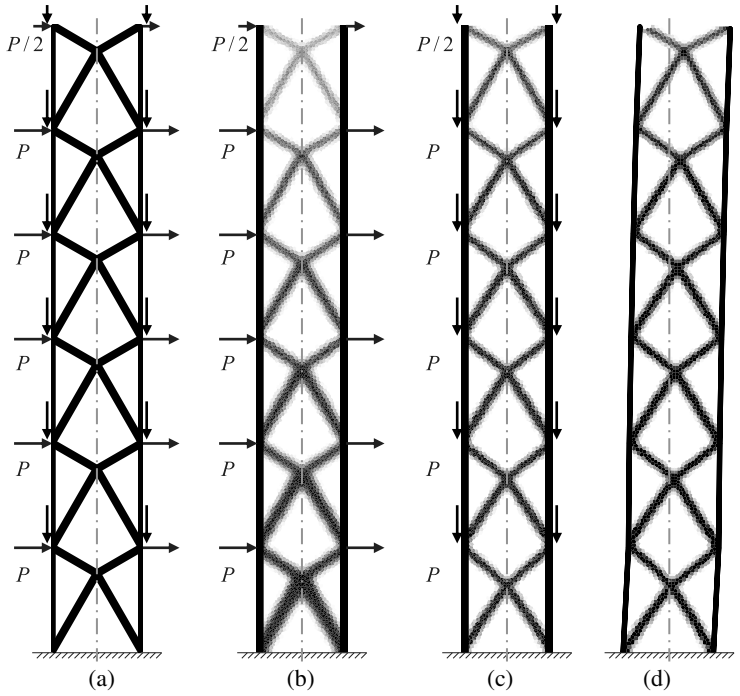

Fig. 6. Topology optimization of a six-module structure: (a) problem statement and discrete solution; (b) compliance; (c and d) buckling and corresponding final critical mode

Table 3. Comparison of Objectives and Cross-Sectional Areas for the Problem in Fig. 6

	Discrete		Discrete/continuum	
	Objective		Objective	
Variable	Compliance	Buckling	Compliance	Buckling
c (MN-m)	10.26	12.19	9.545	10.744
P_{cr}	220.3	262.9	308.59	310.78
A_1 (m^2)	0.6941	0.6477	0.6405	0.6276
A_2 (m^2)	0.4565	0.5133	0.4338	0.4905
A_3 (m^2)	0.2686	0.3559	0.2448	0.3169
A_4 (m^2)	0.1310	0.2012	0.1041	0.1532
A_5 (m^2)	0.0438	0.0765	0.0276	0.0441
A_6 (m^2)	0.0064	0.0119	0.0032	0.0077

more iterations for the optimal geometry to converge than that of compliance.

Concluding Remarks and Extensions

The methodology presented here is useful in determining the optimal geometry of structural systems for high-rise building design, which includes the sizing of the columns throughout the procedure. This approach can be generalized for several other objectives, including compliance, deflection, eigenfrequency, etc. In particular, this work investigated linearized buckling as an objective for the optimization of high-rise buildings. The discrete/continuum framework, originally presented in Stromberg et al. (2012), was extended to simultaneously optimize the cross-sectional areas of the discrete elements and the densities of the continuum (polygonal) elements. As an extension of the work presented here, the incorporation of other objective functions, such as natural frequency, deflection, stress levels, etc., in addition to nonlinearities associated with the buckling problem (i.e., incorporating P-δ and second-order effects) is currently under investigation by the authors.

Acknowledgments

The first author gratefully acknowledges the support form the National Science Foundation (NSF) Graduate Research Fellowship Program (GRFP). The authors also acknowledge support from the NSF under grants CMMI #1234243 and CMMI #1335160, and from the Donald B. and Elizabeth M. Willett endowment at the University of Illinois at Urbana-Champaign. Any opinion, finding, conclusions, or recommendations expressed here are those of the authors and do not necessarily reflect the views of the sponsors.

References

Adams, N., Frampton, K., and van Leeuwen, T. (2012). *SOM journal 7*, Hatje Cantz & Company KG.

Baker, W. F. (1992). "Energy-based design of lateral systems." *Struct. Eng. Int.*, 2(2), 99–102.

Bendsoe, M. P. (1989). "Optimal shape design as a material distribution problem." *Struct. Optim.*, 1(4), 193–202.

Bendsoe, M. P., and Sigmund, O. (1999). "Material interpolation schemes in topology optimization." *Arch. Appl. Mech.*, 69(9–10), 635–654.

Bendsoe, M. P., and Sigmund, O. (2002). *Topology optimization: Theory, methods and applications*, Springer, Berlin, Heidelberg.

Christensen, P. W., and Klarbring, A. (2008). *An introduction to structural optimization*, Springer, New York.

Cook, R. D., Malkus, D. S., Plesha, M. E., and Witt, R. J. (2001). *Concepts and applications of finite element analysis*, 4th Ed., Wiley, New York.

Diaz, A. R., and Kikuchi, N. (1992). "Solutions to shape and topology eigenvalue optimization problems using a homogenization method." *Int. J. Numer. Meth. Eng.*, 35(7), 1487–1502.

Folgado, J., and Rodrigues, H. C. (1998). "Structural optimization with a non-smooth buckling load criterion." *Control Cyber.*, 27(2), 235–253.

Huang, X., and Xie, M. (2010). *Evolutionary topology optimization of continuum structures: Methods and applications*, Wiley, New York.
Kemmler, R., Lipka, A., and Ramm, E. (2005). "Large deformations and stability in topology optimization." *Struct. Multidisc. Optim.*, 30(6), 459–476.
Kosaka, I., and Swan, C. C. (1999). "A symmetry reduction method for continuum structural topology optimization." *Comput. Struct.*, 70(1), 47–61.
LeMessurier, W. J. (1976). "A practical method of second order analysis: Part I—Pin-jointed systems." *Eng. J. AISC*, 13(4), 89–96.
LeMessurier, W. J. (1977). "A practical method of second order analysis: Part II—Rigid frames." *Eng. J. AISC*, 14(2), 49–67.
Martini, K. (2011). "Harmony search method for multimodal size, shape, and topology optimization of structural frameworks." *J. Struct. Eng.*, 10.1061/(ASCE)ST.1943-541X.0000378, 1332–1339.
Min, S., and Kikuchi, N. (1997). "Optimal reinforcement design of structures under the buckling load using the homogenization design method." *Struct. Eng. Mech.*, 5(5), 565–576.
Neves, M. M., Rodrigues, H. C., and Guedes, J. M. (1995). "Generalized topology design of structures with a buckling load criterion." *Struct. Multidisc. Optim.*, 10(2), 71–78.
Neves, M. M., Sigmund, O., and Bendsoe, M. P. (2002). "Topology optimization of periodic microstructures with a penalization of highly localized buckling modes." *Int. J. Numer. Meth. Eng.*, 54(6), 809–834.
Niu, B., Yan, J., and Cheng, G. D. (2008). "Optimum structure with homogeneous optimum cellular material for maximum fundamental frequency." *Struct. Multidisc. Optim.*, 39(2), 115–132.
Olhoff, N., and Du, J. (2012). "On topological design optimization of vibrating structures." Lecture notes from CISM, Udine, Italy.
Olhoff, N., and Rasmussen, S. H. (1977). "On bimodal optimum loads of clamped columns." *Int. J. Solids Struct.*, 13(7), 605–614.
Pedersen, N. L. (2000). "Maximization of eigenvalues using topology optimization." *Struct. Multidisc. Optim.*, 20(1), 2–11.
Rahmatalla, S. F. (2004). "Continuum topology design of sparse structures and compliant mechanisms." Ph.D. thesis, Univ. of Iowa, Iowa City, IA.
Rahmatalla, S. F., and Swan, C. C. (2003). "Form finding of sparse structures with continuum topology optimization." *J. Struct. Eng.*, 10.1061/(ASCE)0733-9445(2003)129:12(1707), 1707–1716.
Rozvany, G. I. N., Zhou, M., and Birker, T. (1992). "Generalized shape optimization without homogenization." *Struct. Multidisc. Optim.*, 4(3), 250–252.
Sekimoto, T., and Noguchi, H. (2001). "Homologous topology optimization in large displacement and buckling problems." *JSME Int. J. Series A*, 44(4), 616–622.
Seyranian, A. P., Lund, E., and Olhoff, N. (1994). "Multiple eigenvalues in structural optimization problems." *Struct. Optim.*, 8(4), 207–227.
Sigmund, O. (2001). "A 99 line topology optimization code written in Matlab." *Struct. Multidisc. Optim.*, 21(2), 120–127.
Stromberg, L. L., Beghini, A., Baker, W. F., and Paulino, G. H. (2012). "Topology optimization for braced frames: Combining continuum and beam/column elements." *Eng. Struct.*, 37, 106–124.
Svanberg, K. (1987). "The method of moving asymptotes—A new method for structural optimization." *Int. J. Numer. Meth. Eng.*, 24(2), 359–373.
Swan, C. C. (2012). "Developing benchmark problems for civil structural applications of continuum topology optimization." *Proc., 20th Anal Comput Specialty Conf.*, ASCE, Reston, VA, 310–322.
Talischi, C., Paulino, G. H., Pereira, A., and Menezes, I. F. M. (2010). "Polygonal finite elements for topology optimization: A unifying paradigm." *Int. J. Numer. Meth. Eng.*, 82(6), 671–698.
Talischi, C., Paulino, G. H., Pereira, A., and Menezes, I. F. M. (2012a). "PolyMesher: A general-purpose mesh generator for polygonal elements written in Matlab." *Struct. Multidisc. Optim.*, 45(3), 309–328.
Talischi, C., Paulino, G. H., Pereira, A., and Menezes, I. F. M. (2012b). "PolyTop: A Matlab implementation of a general topology optimization framework using unstructured polygonal finite element meshes." *Struct. Multidisc. Optim.*, 45(3), 329–357.
Zyczkowski, M., and Gajewski, A. (1988). *Optimal structural design under stability constraints*, Kluwer Academic Press, Dordrecht, Netherlands.